NOTES AND CORRESPONDENCE

Vortex Dipoles for Surface Quasigeostrophic Models

DAVID J. MURAKI

Simon Fraser University, Burnaby, British Columbia, Canada

CHRIS SNYDER

National Center for Atmospheric Research, Boulder, Colorado*

(Manuscript received 22 July 2005, in final form 1 November 2006)

ABSTRACT

A new class of exact vortex dipole solutions is derived for surface quasigeostrophic (sQG) models. The solutions extend the two-dimensional barotropic modon to fully three-dimensional, continuously stratified flow and are a simple model of localized jets on the tropopause. In addition to the basic sQG dipole, dipole structures exist for a layer of uniform potential vorticity between two rigid boundaries and for a dipole in the presence of uniform background vertical shear and horizontal potential temperature gradient. In the former case, the solution approaches the barotropic Lamb dipole in the limit of a layer that is shallow relative to the Rossby depth based on the dipole's radius. In the latter case, dipoles that are bounded in the far field must propagate counter to the phase speed of the linear edge waves associated with the surface temperature gradient.

1. Introduction

Steadily translating dipolar vortices, also known as modons, arise as exact solutions in many geophysical fluid systems (Flierl 1987). They can be viewed as a robust pair of opposite-signed vortices whose mutual interaction leads to steady propagation of the entire structure. Vortex dipoles have been used as models for cold-core oceanic rings (Flierl 1979), atmospheric blocks (McWilliams 1980; Butchart et al. 1989), and troughs and localized jets at the tropopause (Van Tuyl and Young 1982; Hakim 2000; Cunningham and Keyser 2000). Applications to tropopause disturbances have been limited by the fact that, except for Berestov (1979), the available dipole solutions all come from barotropic or layered models. For these applications, the surface quasigeostrophic equations (sQG; Juckes 1994; Held et al. 1995) offer a most natural and simple description of the flow, in which potential vorticity is uniform away from the strong gradients at the tropopause, and the tropopause itself is represented as a rigid boundary. Models based on sQG have been applied extensively to the midlatitude tropopause (Rivest et al. 1992; Juckes 1994; Muraki and Hakim 2001; Hakim et al. 2002). Moreover, vortex dipoles provide useful idealizations of localized jets at the tropopause even when isolated, coherent dipoles are not present, as in a baroclinic wave [e.g., Fig. 4 of Plougonven and Snyder (2005), in which the jet and associated diffluent region downstream of the trough resemble the flow in a vortex dipole]. In this note, we derive a three-dimensional, continuously stratified modon for sQG. This modon is the simplest model for a localized jet on the tropopause that retains realistic vertical structure. Since the troposphere is of finite depth and typically exhibits large-scale temperature gradients, we also extend the basic dipole solution to a fluid layer between two rigid boundaries, and to the presence of uniform background vertical shear and horizontal potential temperature gradient.

* The National Center for Atmospheric Research is sponsored by the National Science Foundation.

Corresponding author address: David J. Muraki, Department of Mathematics, Simon Fraser University, Burnaby, BC V5A 1S6, Canada.
E-mail: muraki@math.sfu.ca

DOI: 10.1175/JAS3958.1

2. The modon construction and the sQG dipole

We consider an atmosphere having infinite horizontal extent (in x, y), bounded below by a rigid lower surface ($z \geq 0$), and under the assumptions of constant stratification and f-plane rotation. The dynamical equations of quasigeostrophy (QG) are advections involving the interior potential vorticity Q and the surface potential temperature Θ^s:

$$\frac{DQ}{Dt} = Q_t + J(\Psi, Q) = 0 \quad \text{and} \tag{1}$$

$$\frac{D\Theta^s}{Dt} = \Theta^s_t + J(\Psi^s, \Theta^s) = 0, \tag{2}$$

where $J(f, g) = f_x g_y - g_x f_y$ is the horizontal Jacobian and superscript s denotes surface ($z = 0$) quantities (Held et al. 1995). The horizontal winds U and V and the potential temperature Θ are given by geostrophy:

$$U = -\Psi_y, \quad V = \Psi_x, \quad \text{and} \quad \Theta = \Psi_z, \tag{3}$$

where the QG streamfunction Ψ is obtained via the three-dimensional Poisson inversion

$$\nabla^2\Psi = Q \quad \text{and} \quad \Psi_z(x, y, 0) = \Theta^s, \tag{4}$$

with decay to uniform flow (specifically in the case of a dipole) imposed in all unbounded directions.

In the literature, the only steady dipole solutions for a three-dimensional, stratified fluid are related to the spherical QG modon of Berestov (1979). The usual starting point for a modon construction is the assumption that the potential vorticity (PV) and streamfunction satisfy one linear relation inside a region of trapped fluid, and a different one outside. For the Berestov dipole the trapped region is a sphere of radius R, and the linear PV–streamfunction relation is

$$Q = \begin{cases} \alpha_i\Psi & \text{inside} \quad (0 \leq r < R) \\ \alpha_o\Psi & \text{outside} \quad (R < r < \infty) \end{cases}, \tag{5}$$

where r is the radial spherical coordinate ($r^2 = x^2 + y^2 + z^2$). The α coefficients are determined as part of the solution process. It is also required that the wind is uniform in the far field. Details of this solution are also given in Flierl (1987). The essential property of the Berestov dipole is that its dynamics are associated entirely with interior PV.

Flows in sQG, in contrast, have uniform PV and their dynamics are associated with a potential temperature disturbance on a horizontal boundary. Thus in sQG, the PV advection equation is satisfied identically by imposing uniform interior PV ($Q = 0$). The dipole motion is then determined solely through the evolution of surface potential temperature (2).

The dipole solution is defined as a localized disturbance propagating steadily with speed $\hat{C}$ along the x axis in a background uniform zonal wind $\hat{U}$. The total streamfunction and potential temperature are expressed as

$$\Psi = \psi(x - \hat{C}t, y, z) - \hat{U}y \quad \text{and} \quad \Theta = \psi_z(x - \hat{C}t, y, z), \tag{6}$$

where the localization of the dipole occurs by enforcing the decay of the disturbances ψ and ψ_z as $r \to \infty$ and $z \to \infty$. The steady-state condition is obtained from the surface advection (2):

$$J(\psi^s + cy, \psi^s_z) = J(\psi^s + cr\sin\phi, \psi^s_z) = 0, \tag{7}$$

where $c = \hat{C} - \hat{U}$ is the flow-relative dipole speed and (r, ϕ) are cylindrical coordinates in the moving frame: $x - \hat{C}t = r\cos\phi$ and $y = r\sin\phi$. The modon construction satisfies the condition (7) by specifying the linear relation

$$\psi^s_z = \begin{cases} -\dfrac{\alpha}{R}(\psi^s + cr\sin\phi) & \text{inside} \quad (0 \leq r < R) \\ 0 & \text{outside} \quad (R < r < \infty) \end{cases}, \tag{8}$$

where zero surface potential temperature outside the dipole radius R is necessary for the decay of ψ as $r \to \infty$. A more general relation, following (5) from Berestov, is discussed in section 4.

The sQG dipole solution is thus obtained by solving the linear system that consists of the zero PV Laplace inversion:

$$\nabla^2\psi = 0, \tag{9}$$

with the modon relation (8) as a surface boundary condition, plus far-field decay. There is an additional consistency relation requiring that the circle defining the region of fluid trapped within the dipole ($r = R$) be itself a streamline of the flow—this determines the proportionality constant α and embodies the only nonlinear aspect of the solution method.

The inhomogeneous contribution in the dipole equation in (8) has a $\sin\phi$ angular dependence. It follows that the streamfunction ψ must inherit the same azimuthal structure. The general solution of the Laplace equation in (9) for this azimuthal structure has the integral representation

$$\psi(r, \phi, z) = Rc\sin\phi \int_0^\infty \hat{\psi}(\sigma) J_1(\sigma r/R) \exp(-\sigma z/R)\sigma \, d\sigma, \tag{10}$$

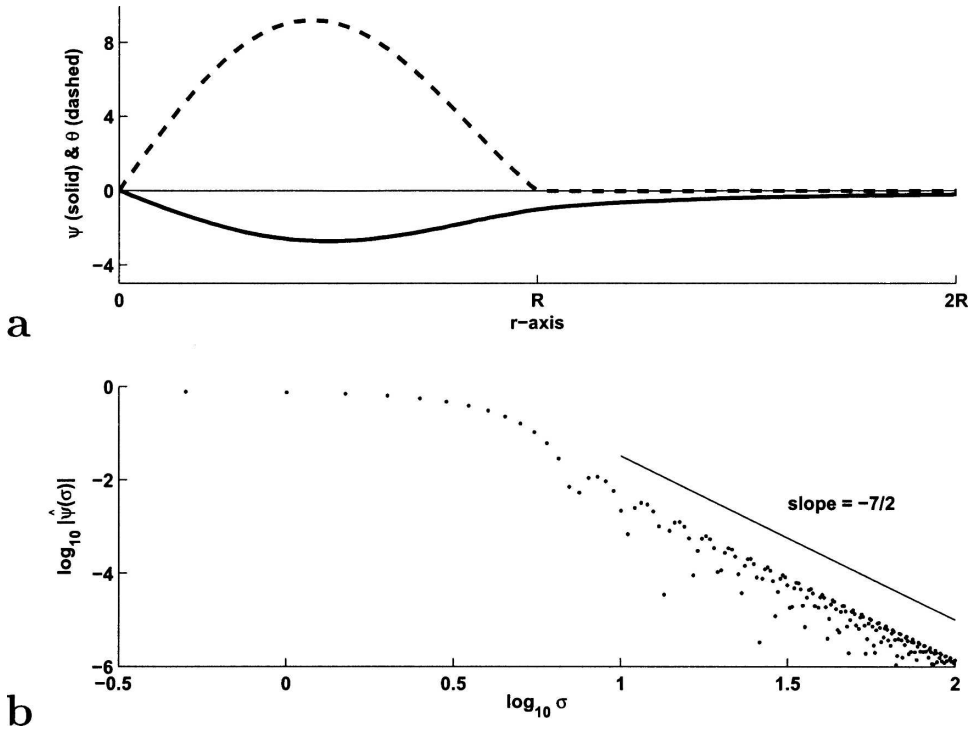

FIG. 1. (a) Radial profiles of disturbance streamfunction (solid line) and potential temperature (dashed line) for the basic dipole. The basic dipole streamfunction is scaled on Rc, and the potential temperature is scaled on c. (b) Log–log scatterplot of Fourier–Bessel amplitudes $\hat{\psi}(\sigma)$ as numerically computed from (11).

where $J_1()$ is the Bessel function of order 1 and $\hat{\psi}(\sigma)$ is a Fourier–Bessel coefficient to be determined from the surface boundary condition. The above integral is known as a Hankel transform and has many properties analogous to the Fourier integral, including an inverse transform (Morse and Feshbach 1953). Substituting the integral representation (10) into the modon condition (8) and applying the inverse transform yields a linear integral equation for the coefficient $\hat{\psi}(\sigma)$:

$$A(\sigma)\hat{\psi}(\sigma) = \alpha\left[\int_0^\infty K(\overline{\sigma}, \sigma)\hat{\psi}(\overline{\sigma})\overline{\sigma}\, d\overline{\sigma} + F(\sigma)\right], \quad (11)$$

which is a standard form known as a Fredholm integral equation of the second kind (Kondo 1991). Details of the derivation are deferred to the appendix. The coefficient $A(\sigma)$, kernel $K(\overline{\sigma}, \sigma)$, and forcing $F(\sigma)$ are given by the expressions

$$A(\sigma) = \sigma,$$

$$K(\overline{\sigma}, \sigma) = \int_0^1 J_1(\overline{\sigma}s)J_1(\sigma s)s\, ds, \quad \text{and}$$

$$F(\sigma) = \int_0^1 J_1(\sigma s)s^2\, ds, \quad (12)$$

where these integrals are evaluated exactly using standard Bessel identities (see the appendix). The coefficient $A(\sigma)$ will be the vehicle for generating the dipole variations of sections 3 and 4.

Numerical solutions for $\hat{\psi}(\sigma)$ given α are simply obtained by matrix inversion after approximating the integral in (11) by a discrete quadrature (such as Simpson's rule) over a sufficiently large interval ($0 \le \sigma \le \Sigma$). Radial profiles of the surface streamfunction (solid line) and potential temperature (dashed line) are shown in Fig. 1a. The Fourier–Bessel spectral amplitudes $\hat{\psi}(\sigma)$ are shown in Fig. 1b (100 of 512 modes shown; $\Sigma = 256$). The line indicates an asymptotic slope of $-7/2$, which is the characteristic (Fourier–Bessel) spectral decay expected when the θ field has a jump in the radial derivative.

The value $\alpha \approx 4.1213$ is found by a simple root-finding procedure that enforces the modon boundary ($r = R$) to be a separating streamline ($\Psi^s = 0$). This feature of the solution is apparent in the total streamfunction $\Psi(x, y, 0)$ shown in Fig. 2. As with other modons, the dipole's propagation speed is simply proportional to its amplitude. A positive value of c makes the upper part of the dipole (Fig. 2) a warm, cyclonic anomaly, which results in a modon that propagates eastward relative to background winds.

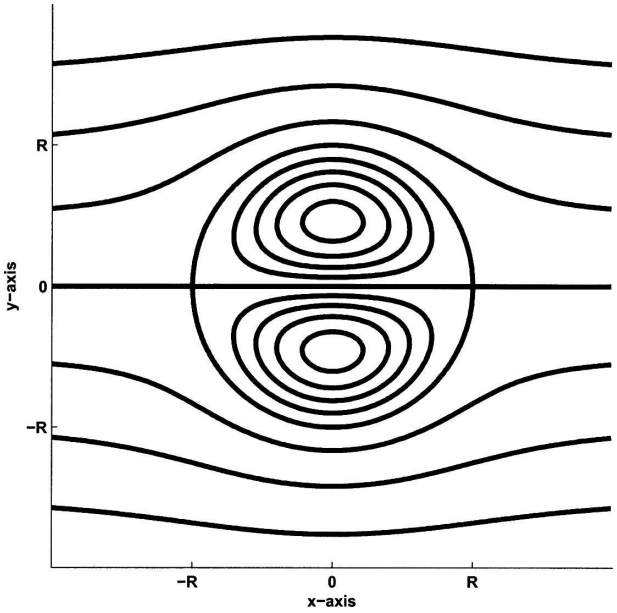

FIG. 2. Contours of the full streamfunction for the basic dipole in a frame in which the dipole is steady. The contour intervals are $Rc/2$. Positive values of c correspond to an easterly incident wind.

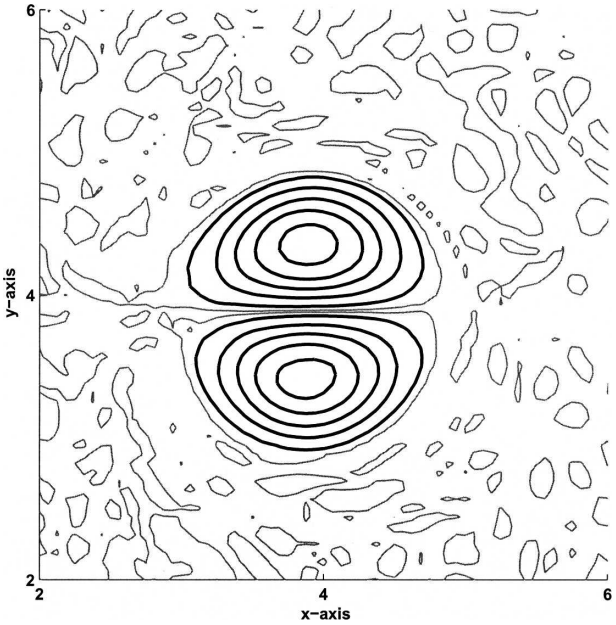

FIG. 3. Contours of the full surface potential temperature for an sQG simulation of the basic dipole that has been initialized with small-scale noise. Despite the noisy background, the dipole has very nearly returned to its center location after one transversal of the periodic domain. The interval of the dark contours is 0.2 of $\theta^s_{\max}$, and the light contours are at ± 0.02 of $\theta^s_{\max}$.

For a variety of flow systems, the stability of dipoles has been inferred through time-dependent simulations (Flierl 1987). We have verified that the propagation and spatial structure for the sQG dipole, and the variants that follow, are robust within the sQG dynamics to the addition of noise into the initial condition. The numerical sQG simulation uses a dealiased pseudospectral method, described in Hakim et al. (2002), and includes weak ∇^8 hyperdiffusion. Unlike the analytic sQG dipole, the numerical simulations assume periodicity in both horizontal directions.

Figure 3 shows contours of θ^s at $t = 8$ from a simulation beginning from an sQG dipole ($c = 1$; $R = 1$) with superimposed initial noise in θ^s. The simulation uses 256^2 collocation points, a domain of size $L = 8$, and initial Gaussian noise that is uncorrelated in space and has variance that is 5% of the dipole's maximum θ^s. Even after propagating a distance of nearly 8, or one complete circuit of the periodic domain, the dipole's structure is little changed from the analytic solution. Longer simulations reveal similar, stable behavior.

3. Dipole in a finite layer

If the sQG dipole is to be a model for localized jets at the tropopause, a natural question is how the finite depth of the troposphere affects the solution. The sQG formalism can be extended to a geometry that includes a constant potential temperature upper lid at height H. Still assuming uniform PV, the analog of the general Laplace solution (10) for the layer involves only a change to the vertical profile in the integral

$$\psi(r, \phi, z) = Rc \sin\phi \int_0^\infty \hat{\psi}(\sigma) J_1(\sigma r/R) \frac{\cosh[\sigma(H - z)/R]}{\cosh(\sigma H/R)} \sigma \, d\sigma, \tag{13}$$

so that $\theta = \psi_z = 0$ at $z = H$. The normalization in the denominator (13) is designed to recover exactly the basic dipole form (10) in the deep-layer limit ($H/R \to \infty$). This change to the vertical mode structure introduces only a minor difference to the left-hand side of the integral equation in (11) in the form of the coefficient

$$A(\sigma) = \sigma \tanh(\sigma H/R). \tag{14}$$

The streamfunction for the finite-depth dipole differs only slightly from the basic dipole (Fig. 2). For a fixed propagation speed c, however, the proportionality constant α does vary significantly with the inverse aspect ratio R/H, as does maximum potential temperature $\theta^s_{\max}$ normalized by the deep-layer value. Figure 4a shows the computed values for α and normalized $\theta^s_{\max}$ as functions of R/H. In the deep-layer limit $R/H \to 0$, the value $\alpha = 4.1213$ of section 2 is recovered. In the

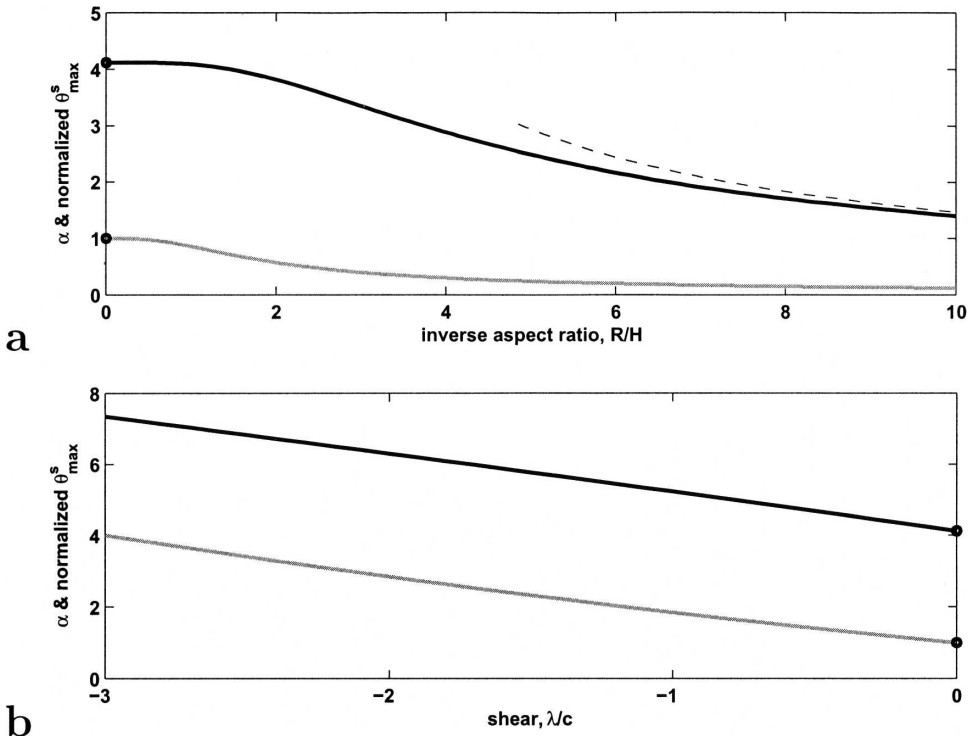

FIG. 4. Variation of the α parameter (thick solid line) for the two dipole variants: (a) finite layer and (b) vertical shear. The thin-layer ($H/R \to 0$) asymptote is shown (thin dashed line) in (a). Also shown in both panels (gray solid line) is the variation of $\theta^s_{\max}$ normalized onto the basic dipole of section 2 ($\theta^s_{\max} \approx 9.24$).

opposite limit of a very thin layer ($R/H \to \infty$), the computed α asymptotically approaches the barotropic value of $(z_1)^2 H/R$ that is indicated in Fig. 4a [$z_1 \approx 3.8317$ is the first zero of the $J_1()$ Bessel function]. This asymptotic value is obtained from the derivation of the barotropic Lamb dipole (Lamb 1945; Meleshko and van Heijst 1994) whose streamfunction has the formula

$$\psi(r, \phi, 0) \to \begin{cases} Rc \sin\phi \left[\dfrac{2}{z_1} \dfrac{J_1(z_1 r/R)}{J_0(z_1)} - \dfrac{r}{R} \right] & \text{inside } (0 \le r < R) \\ Rc \sin\phi \left(-\dfrac{R}{r} \right) & \text{outside } (R < r < \infty) \end{cases}. \tag{15}$$

As an additional check (not shown), the computed streamfunction (13) itself was verified to approach the above Lamb solution with decreasing H.

This observation illustrates the general principle that, in sQG, the horizontal scales whose Rossby heights are deeper than the layer behave roughly as those of the barotropic vorticity equation. The decrease of the normalized $\theta^s_{\max}$, seen in Fig. 4a, corresponds to the fact that, as the layer thins, weaker potential temperature disturbances are required to maintain a fixed velocity perturbation.

4. Dipole in a horizontal temperature gradient

The midlatitude troposphere typically has significant baroclinicity. A background environment with a horizontal temperature gradient and vertical shear can be incorporated without introducing interior PV by adding a constant vertical shear of magnitude λ to the full streamfunction:

$$\Psi = \psi(x - \hat{C}t, y, z) - (\hat{U} + \lambda z) y \quad \text{and}$$
$$\Theta = \psi_z(r, \phi, z) - \lambda y. \tag{16}$$

This modifies the surface potential temperature condition

$$0 = J(\psi^s + cy, \psi^s_z - \lambda y) = J\left(\psi^s + cy, \psi^s_z + \frac{\lambda}{c} \psi^s \right). \tag{17}$$

The second Jacobian form in (17) is obtained by replacing its second argument by a linear combination of the

original arguments, since $J(f, g) = J[f, g + (\lambda/c)f]$. The linear modon relation in cylindrical coordinates with respect to the moving frame is now

$$\psi^s_z + \frac{\lambda}{c}\psi^s = \begin{cases} -\dfrac{\alpha}{R}(\psi^s + cr\sin\phi) & \text{inside } (0 \le r < R) \\ 0 & \text{outside } (R < r < \infty) \end{cases}, \tag{18}$$

where again the zero exterior condition ensures far-field decay of the disturbance streamfunction ψ. Using the same integral representation as (10), the change to the integral equation again involves the left-hand-side coefficient

$$A(\sigma) = \left(\sigma - \frac{\lambda}{c}\right). \tag{19}$$

For positive shear and westward propagation ($\lambda > 0$; $c < 0$), the left-hand-side factor $A(\sigma)$ is strictly positive for $0 \le \sigma < \infty$ and numerical solution of (11) proceeds uneventfully. The dependence of α and normalized $\theta^s_{\max}$ against $\lambda/c < 0$ is shown in Fig. 4b. These dipoles in shear have been observed to evolve stably in time-dependent sQG simulations.

The Ψ–Θ relation (18) is equivalent to beginning as in the general Berestov construction (5) with an α_i and α_o in (8). To see this, note first that nonzero α_o implies that the disturbances Ψ^s and ψ^s_z as defined in (6) can no longer be vanishing at $r \to \infty$. Rather, it is necessary to introduce the Eady shear as in (16) with $\alpha_o/R = \lambda/c$. The result can then be rewritten in the form (18). The zero exterior condition of (18) is required mathematically as the Hankel transform can only be applied for disturbances that decay as $r \to \infty$.

For positive shear and eastward propagation ($\lambda > 0$; $c < 0$), unsuccessful attempts to solve numerically the integral equation suggest that a singularity in the amplitude $\hat{\psi}(\sigma)$ develops where the factor $A(\sigma)$ is zero. This critical value, $\sigma_c = \lambda/c > 0$, represents the scale at which the propagation speed and vertical decay scale exactly match those of the family of edge waves with horizontal wavenumber σ_c/R. We associate this singularity to a resonance with the edge waves. A precedent for such an interpretation is provided by the eastward propagating dipoles on the sphere constructed by Verkley (1987). These dipoles, in a barotropic vorticity model, have a composite structure consisting of a central dipole coupled to a far field of standing Rossby–Haurwitz waves. A similar object occurring within the sQG dynamics is the exact, standing-wave solution

$$\psi(r, \phi, z) = J_1(\sigma_c r/R)\sin\phi\exp(-\sigma_c z/R), \tag{20}$$

which satisfies the far-field condition (18) everywhere on the $z = 0$ surface. In contrast to the dipole in the spherical geometry, this sQG solution requires incoming Rossby waves from infinity to conspire precisely with their outgoing radiation to form the steady interference pattern.

5. Conclusions

Vortex dipoles are the simplest idealization of a localized jet at the tropopause, yet existing dipole solutions pertain only to barotropic or layered models or to dipoles with significant anomalies of interior PV. We have developed a vortex-dipole solution for sQG that is more appropriate to tropopause disturbances, in that its dynamics are driven only by potential temperature advection on a single surface (approximating the tropopause) yet its vertical structure extends continuously into the uniform-PV interior. Rather than the algebraic conditions produced by matching across the dipole's boundary in other dipole solutions, the sQG dipole requires the solution of the three-dimensional Laplace equation and yields an integral equation for the coefficient in the ψ–θ relation within the dipole. The basic sQG modon can also be extended to a troposphere of finite depth with uniform potential temperature at the lower boundary, and to the presence of uniform background vertical shear and horizontal potential temperature gradient. Numerical simulations with the pseudospectral sQG model of Hakim et al. (2002) indicate that the basic sQG dipole, and the variants presented here, are robust to initial background noise. However, we are currently investigating the nature and stability of similar dipole solutions for the primitive equations, in particular for their interaction with inertia–gravity waves. Other modifications not included in this Note include a superimposed monopolar rider and an sQG dipole in the presence of planetary vorticity gradients. The construction technique also likely allows extension to weak shear (Swenson 1986), tropopause deformation (Rivest et al. 1992), and possibly, beyond QG corrections (Muraki et al. 1999).

Acknowledgments. DJM gratefully acknowledges support through NSF DMR-9704724, NSERC RGPIN238928, the Alfred P. Sloan Foundation, and the Visitor Program of the Mesoscale and Microscale Meteorology Division at NCAR. Author CS was partially supported by NSF Grant CMG-0327582. We are indebted to Andreas Dörnbrack for alerting us to the paper of Meleshko and van Heijst. Last, special thanks are given to Greg Hakim and Phil Cunningham for their enthusiastic support of this analytical work.

APPENDIX

Details of the Integral Equation

The derivation of the integral equation in (11) relies on the integral relations between $\psi(s)$ and its Hankel transform $\hat{\psi}(\sigma)$:

$$\psi(s) = \int_0^\infty \hat{\psi}(\sigma) J_m(\sigma s)\sigma \, d\sigma \quad \text{and}$$

$$\hat{\psi}(\sigma) = \int_0^\infty \psi(s) J_m(\sigma s) s \, ds, \tag{A1}$$

where m is any nonnegative integer index (Morse and Feshbach 1953). The second integral thus corresponds to the inversion formula that obtains the $\hat{\psi}(\sigma)$ coefficient for the integral representation of $\psi(s)$. Substitution of the integral representation (10) into the modon relation (8) at $z = 0$ gives

$$-\int_0^\infty \overline{\sigma}\hat{\psi}(\overline{\sigma}) J_1(\overline{\sigma}s)\overline{\sigma} \, d\overline{\sigma} = -\alpha \mathcal{H}(1-s)\left[\int_0^\infty \hat{\psi}(\overline{\sigma}) J_1(\overline{\sigma}s)\overline{\sigma} \, d\overline{\sigma} + s\right], \tag{A2}$$

where $s = r/R$ and $\mathcal{H}(1 - s)$ denotes the Heaviside step function, which is zero for $s > 1$. Note also that in (A2) the (dummy) variable of integration has been replaced with $\overline{\sigma}$. Multiplying the above by $s\,J_1(\sigma s)$ and integrating from $s = 0 \to \infty$ results in the integral equation in (11). Note that the finite limits of the integrals for the kernel and forcing (12) are a consequence of the vanishing of the Heaviside factor for $s > 1$ (after interchanging the order of the right-hand-side integrals). The Bessel integrals for the kernel and forcing (12) are given explicitly by

$$K(\overline{\sigma}, \sigma) = \begin{cases} \dfrac{\overline{\sigma} J_1(\sigma) J_0(\overline{\sigma}) - \sigma J_1(\overline{\sigma}) J_0(\sigma)}{\sigma^2 - \overline{\sigma}^2} & \text{for} \quad \overline{\sigma} \neq \sigma \\ \dfrac{[J_1(\sigma)]^2 - J_0(\sigma) J_2(\sigma)}{2} & \text{for} \quad \overline{\sigma} = \sigma \end{cases} \quad \text{and}$$

$$F(\sigma) = \frac{J_2(\sigma)}{\sigma}. \tag{A3}$$

REFERENCES

Berestov, A. L., 1979: Solitary Rossby waves. *Izv. Acad. Sci. USSR, Atmos. Oceanic Phys.,* **15,** 443–447.

Butchart, N., K. Haines, and J. C. Marshall, 1989: A theoretical and diagnostic study of solitary waves and atmospheric blocking. *J. Atmos. Sci.,* **46,** 2063–2078.

Cunningham, P., and D. Keyser, 2000: Analytical and numerical modelling of jetstreaks: Barotropic dynamics. *Quart. J. Roy. Meteor. Soc.,* **126,** 3187–3217.

Flierl, G. R., 1979: A simple model for warm and cold core rings. *J. Geophys. Res.,* **84,** 57–65.

——, 1987: Isolated eddy models in geophysics. *Annu. Rev. Fluid Mech.,* **19,** 493–530.

Hakim, G. J., 2000: Climatology of coherent structures on the extratropical tropopause. *Mon. Wea. Rev.,* **128,** 385–406.

——, C. Snyder, and D. J. Muraki, 2002: A new surface model for cyclone–anticyclone asymmetry. *J. Atmos. Sci.,* **59,** 2405–2420.

Held, I. M., R. T. Pierrehumbert, S. T. Garner, and K. L. Swanson, 1995: Surface quasigeostrophic dynamics. *J. Fluid Mech.,* **282,** 1–20.

Juckes, M., 1994: Quasigeostrophic dynamics of the tropopause. *J. Atmos. Sci.,* **51,** 2756–2768.

Kondo, J., 1991: *Integral Equations.* Clarendon, 466 pp.

Lamb, H., 1945: *Hydrodynamics.* Dover, 738 pp.

McWilliams, J. C., 1980: An application of equivalent modons to atmospheric blocking. *Dyn. Atmos. Oceans,* **5,** 43–66.

Meleshko, V. V., and G. J. F. van Heijst, 1994: On Chaplygin's investigations of two-dimensional vortex structures in an inviscid fluid. *J. Fluid Mech.,* **272,** 157–182.

Morse, P. M., and H. Feshbach, 1953: *Methods of Theoretical Physics.* Vol. 1. McGraw-Hill, 997 pp.

Muraki, D. J., and G. J. Hakim, 2001: Balanced asymmetries of waves on the tropopause. *J. Atmos. Sci.,* **58,** 237–252.

——, C. Snyder, and R. Rotunno, 1999: The next-order corrections to quasigeostrophic theory. *J. Atmos. Sci.,* **56,** 1547–1560.

Plougonven, R., and C. Snyder, 2005: Gravity waves excited by jets: Propagation versus generation. *Geophys. Res. Lett.,* **32,** L18802, doi:10.1029/2005GL023730.

Rivest, C., C. A. Davis, and B. F. Farrell, 1992: Upper-tropospheric synoptic-scale waves. Part I: Maintenance as Eady normal modes. *J. Atmos. Sci.,* **49,** 2108–2119.

Swenson, M., 1986: Equivalent modons in simple shear. *J. Atmos. Sci.,* **43,** 3177–3185.

Van Tuyl, A. H., and J. A. Young, 1982: Numerical simulation of nonlinear jet streak adjustment. *Mon. Wea. Rev.,* **110,** 2038–2054.

Verkley, W. T. M., 1987: Stationary barotropic modons in westerly background flows. *J. Atmos. Sci.,* **44,** 2383–2398.